Int. J. Electrochem. Sci., 14 **(2019)** 8624 – 8638, doi: 10.20964/2019.09.43

International Journal of
ELECTROCHEMICAL
SCIENCE
www.electrochemsci.org

Short Communication

Microstructure of Passive Film on Steel in Synthetic Concrete Pore Solution in Presence Chloride and Nitrite

Xiaozhen Li, Junzhe Liu[*]*, Jianmin Wang, Jundi Geng*

NingBo University, Faculty of Architectural, Civil Engineering and Environment, Ningbo, Zhejiang 315211, China
[*]E-mail: liujunzhe@nbu.edu.cn

Received: 5 May 2019 / *Accepted:* 24 June 2019 / *Published:* 31 July 2019

Microscopic characteristics of passive films on steel surfaces under three corrosion conditions—chloride, carbonated and compound solutions—were studied by X-ray photoelectron spectroscopy (XPS) and X-ray diffraction (XRD). The influence of $n(NO_2^-)/n(Cl^-)$ on the corrosion current was evaluated by the anodic polarization method. Experiments revealed that nitrite expanded the range of steel bar passivation and effectively prevented steel bar corrosion caused by chloride ions. The results showed that in the simulated chloride solution, a complete passivation film was formed on the surface of the steel wafers under the condition of $n(NO_2^-)/n(Cl^-)=1.5$. In the simulated carbonated solution, when the content of sodium nitrite was 3%, the passivation film on the surfaces of steel wafers was completely formed. Steel corrosion was substantial in the compound solution, and the passivation effect was obvious when $n(NO_2^-)/n(Cl^-)=2.0$. With the addition of sodium nitrite, the main components of the passivation film were FeOOH, FeO and Fe_3O_4. In the outer layer, FeOOH was the main component, whereas FeO and Fe_3O_4 were found in relatively lower proportions. The inner layer was relatively dense because FeO and Fe_3O_4 were the main components. Sodium nitrite can increase the forward reaction rate of passivation film formation, and the thickness of passivation film can be controlled by changing the content of the reaction material. After a complete passivation film was formed on the surface of the steel, further reaction between the "external" material and the elemental iron inside the passivation film was hindered. $(NaFeO_2)_2$ in the solution was easily hydrolyzed in water to form FeOOH, which precipitated and accumulated on the outer layer of the passivation film to form the "double-layer structure".

Keywords: chloride; carbonation; nitrite; passive film; microstructure

1. INTRODUCTION

Concrete pore fluid is in a highly alkaline state under normal conditions, resulting in a dense passivation film on the surface of steel reinforcement. Both carbon dioxide diffusion and chloride

erosion will cause changes in pH [1-4], which affects the stability of the passivation film, leading to corrosion of the steel reinforcement and the deterioration of reinforced concrete structures. Therefore, the corrosion resistance of steel mainly depends on the nature of the passivation film [5]. The prevention and treatment of steel corrosion can be solved by sealing materials, compound alkalization, cathodic protection and rust inhibitors [6]. Inhibitors have been widely used due to their low cost and efficiency [7-10].

Results in the literature indicate that nitrite inhibitors could increase the critical chloride ion concentration and inhibit the corrosion of rebar [7, 11]. Although the nitrite content that inhibited the corrosion of steel bars has been studied, researchers have reported different results [12-14]. This discrepancy is partly due to the complexity of the concrete environment and partly due to the factors that affect the failure of a passivation film, including the surface state, alloy and phase composition, as well as the concrete permeability, chloride concentration, solution pH, temperature and humidity. Pitting susceptibility was studied in nitrite chloride containing solution [5]. The behavior and efficiency of nitrite on mechanical strength and porosity in the presence of CO_2 and chloride was evaluated [9]. The characteristics of passivation films are affected by the polarization potential, polarization time and ion concentration in the medium, while these factors are related to the microstructural characteristics of the passivation film. Steel corrosion is ultimately caused by changes in the composition and structure of the passivation film [15-16]. Therefore, it is an important task to clarify the failure process of a passivation film under the action of carbonation and chlorine salt corrosion with nitrite ions to improve the environment of the steel bar surface in concrete. However, there are few reports on these issues.

This paper focuses on the composition of a steel passivation film in concrete pore solution in the presence of chloride, nitrite and carbonation [17] and studies the effect of nitrite on steel under different corrosion environments. Herein, X-ray photoelectron spectroscopy and X-ray diffractometry are used to examine the microstructural composition and evolution rules of steel passivation films in three corrosive environments, providing a theoretical basis for the optimization of steel surface passivation film composition and the improvement of steel rust resistance. The influence of $n(NO_2^-)/n(Cl^-)$ on the corrosion current was evaluated by the anodic polarization method.

2. MATERIALS AND METHODS

2.1. Steel sample preparation

A steel bar with a diameter of 10 mm was cut into sections 50 mm in length that had the passivation film removed. Each steel bar was polished with a sequence of 80 grit, 100 grit, and 150 grit sandpapers to be a bright mirror finish and then cut into 2 mm thick round pieces using the linear cutting method. The chemical composition of the steel is shown in Table 1.

Table 1. Chemical composition of the steel bar/%

Element	C	Si	Mn	P	S	Cr	Ni	Mo
Content	0.228	0.310	1.340	0.029	0.020	0.084	0.040	0.016

2.2 Pore solution with nitrite preparation

Two types of simulated pore solutions were prepared according to the proportions shown in Table 2.

Table 2. Ratios of the simulated concrete pore solutions

Classification	Pore solution before carbonation			Pore solution after carbonation	
Reagent	$Ca(OH)_2$	NaOH	KOH	Na_2CO_3	$NaHCO_3$
mol/L	0.001	0.2	0.6	0.0015	0.03

Chloride pore solution: Considering forming a passivation film in the chloride pore solution, 0.8 mol/L $NaHCO_3$ was added to adjust the pH to 13.3. NaCl and $NaNO_2$ were added into the solution to adjust the Cl^- content to 0, 0.1%, 0.5%, 1.0%, 2%, and 4% and $n(NO_2^-)/n(Cl^-)$ to 0.5, 1.0, and 1.5.

The influence of $n(NO_2^-)/n(Cl^-)$ on the corrosion current was evaluated by the anodic polarization method. Electrolytes with different molar ratios are shown in Table 3. A PS-6 steel corrosion measuring instrument and a saturated calomel electrode were used. A steel bar with a superficial area of 1 cm^2 was used as the electrode; the passivation film and grease on the bar were removed with sandpaper and acetone. The instrument was preheated for 15 minutes to stabilize the instrument before measuring. The current and potential were measured at the kinetic potential change of 50 mV/min.

Table 3. Ratios of the simulated concrete pore solutions for the anodic polarization test

Type	$NaNO_2$(%)	NaCl(%)	$n(NO_2^-)/n(Cl^-)$
A	0	0	0
B	0	1.0	0
C	0.1	1.0	0.085
D	0.2	1.0	0.17
E	0.4	1.0	0.34
B’	0	2.0	0
C’	0.3	2.0	0.13
D’	0.7	2.0	0.3
E’	1.0	2.0	0.42

Carbonated pore solution: Note that 1%, 2% and 3% sodium nitrite were added to the pore solution after carbonation.

Compound solutions of carbonation and chloride: NaCl and $NaNO_2$ were added to the pore solution after carbonation to adjust the Cl^- content to 0.5% and 1.0% and $n(NO_2^-)/n(Cl^-)$ to 0.5, 1.0, 1.5, and 2.0.

Three steel wafers were added to the above solutions and were observed every month. The surfaces of the wafers were preliminarily determined by visual inspection. After three months, the wafers in the solutions were removed and used as test samples.

2.3 Test sample selection

In a chloride pore solution with a Cl^- content of 1%, the steel surfaces showed different degrees of corrosion. In the solution with a Cl^- content of 0.5% and $n(NO_2^-)/n(Cl^-)$ of 0.5, the surface of the steel had a certain depth of corrosion characteristics with some pitting corrosion. In the solution with a Cl^- content of 0.5% and $n(NO_2^-)/n(Cl^-)$ of 1.0, only a small amount of yellow speckled rust appeared on the surface of the steel. In the solution with a Cl^- content of 0.5% and $n(NO_2^-)/n(Cl^-)$ of 1.5, there was no rust on the surface of the steel, indicating that a stable passivation film had been generated and can be used as a test sample.

In the carbonated pore solution, the steel wafers in a 1% sodium nitrite solution were corroded and were not taken as samples. The surfaces of the steel wafers doped with 2% sodium nitrite solution showed a gray-white rust-free state; therefore, these wafers can be used as test samples.

The corrosion of the steel wafers in the compound solution was the most serious. In the solution with 1.0% chloride and $n(NO_2^-)/n(Cl^-)$ less than or equal to 0.5, there were yellow filamentous corrosion materials on the surfaces of the steel wafers. These materials detached from the surface of steel and floated in the solution. The best passivation effect was found in the steel wafers in 0.5% chloride and $n(NO_2^-)/n(Cl^-)$ less than or equal to 2.0. There was no rust on the surface of these wafers. In this paper, steel wafers subjected to a chloride solution with 0.5% Cl^- and 1.5 $n(NO_2^-)/n(Cl^-)$, a carbonated solution with 2% sodium nitrite, and a compound solution with 2.0 $n(NO_2^-)/n(Cl^-)$ were chosen as the test samples. The microstructures of the passive films of these wafers were analyzed by XPS and XRD. A total of 300 ml of the three types of previously prepared simulated pore solutions were poured into three covered glass flasks. Two of the steel wafers prepared above were then added into each flask, and the flask was tightly sealed with a cap. After 6 months, the steel wafers in the solutions were washed with deionized water and acetone and then stored in a container filled with Ar after drying. The samples were analytically tested by X-ray diffraction (XRD) and X-ray photoelectron spectroscopy (XPS) within two hours after preparation.

2.4 Test parameter setting

A Mg target was used for XPS. The X-ray emission current was 20 mA, and the source voltage was 10 kV. The multiplier voltage was 2.8 kV. The full spectrum passing energy was 100 eV. The

narrow scan passing energy was 50 eV. A total of 20 scans were performed, and each step took 10 ms. The samples were sputtered for 5 s by Ar+ at a speed of 3 nm/min to eliminate the effect of contaminators. After the XPS was tested at 0 nm and 5 nm, CasaXPS2.3.16 was used for the peak fitting analysis of the data. The peak curves of all elements were calibrated with C1s, and the calibration value was 284.6 eV with the combined energy.

The XRD equipment used in this study was D8 Advance Davinci (produced by the Bruker company in Germany). The device used a K1 ray, and the device had a tube voltage and current of 40 kV and 40 mA, respectively. The device scanned continuously with a scanning range of 20~70 ° at a scan rate of 8 °/min; the step length was 0.02°.

3. RESULTS AND DISCUSSION

3.1. Microscopic characteristics of the passivation substance in the chloride solution

3.1.1 XPS full-scan of the passivation substance in the chloride solution

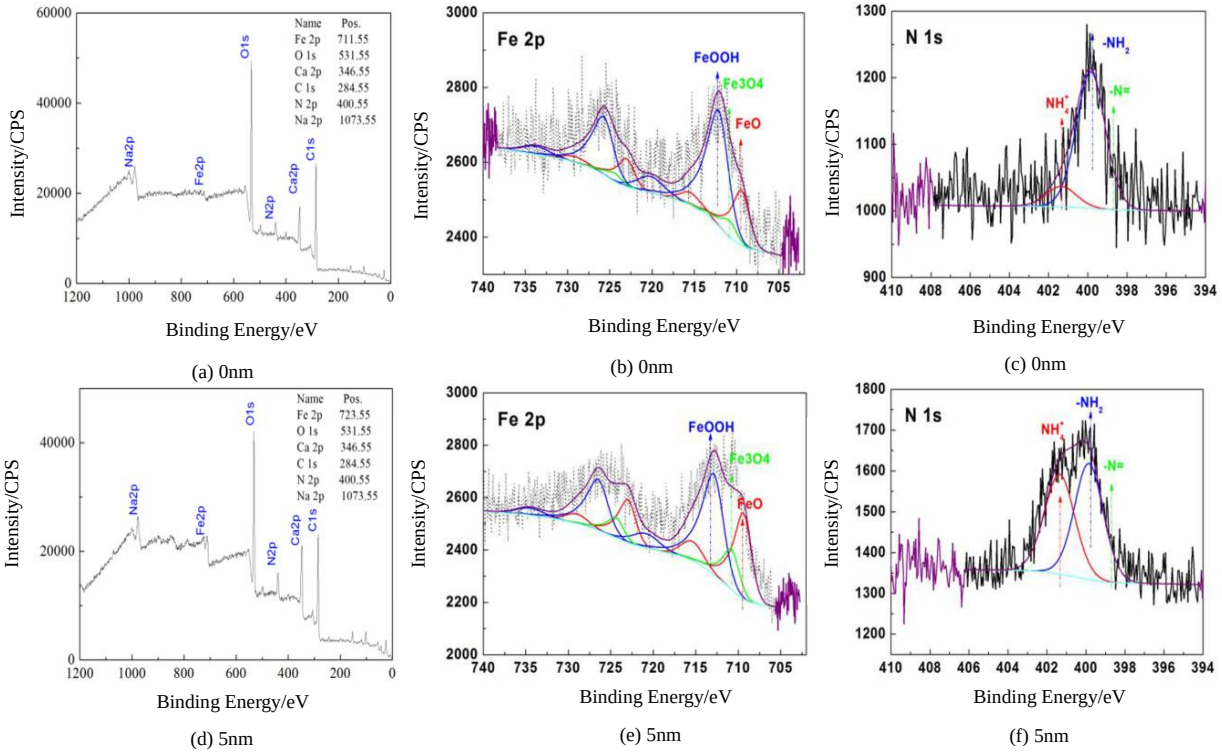

Figure 1. XPS full-scan spectrum diagrams showing Fe and N of the passivation film in the simulated chloride solution at positions of 0 nm and 5 nm ($n(NO_2^-)/n(Cl^-)=1.5$)

Figures 1 (a) and (d) are the XPS full-scan spectrum diagrams of the steel wafers in chloride solution with nitrite at the positions of 0 nm and 5 nm. The main compositions of the steel passivation film at 0 nm and 5 nm are Fe, O, C and Cl. The carbon peak appears in the XPS of the chloride solution, but there is no C element in the solution. According to the analysis, the carbon element comes

from the steel bar itself. The binding energies of Fe 2p at 0 nm and 5 nm in the chloride solution are 711.55 eV and 723.55 eV, respectively.

3.1.2 XPS scanning images of Fe and N of the passivation film in the chloride solution

Figures 1 (b) and (e) are fitted by Casa XPS software to obtain the XPS scanning images of Fe and N in the passivation film with 0.5% chloride and 1.5 $n(NO_2^-)/n(Cl^-)$. The spectrum of Fe 2p is bimodal because its orbit spins split into two energy levels (Fe 2p 1/2 and Fe 2p 3/2). Figure 1 (b) shows the XPS spectrum of Fe at 0 nm and is mainly composed of FeOOH, FeO and Fe_3O_4. This finding is consistent with the existing literature research results [13]. As seen from the XPS peak fitting data of Fe in Table 4, the ratios of FeOOH, FeO and Fe_3O_4 are 66.2%, 28.4%, and 5.4%, respectively, indicating that the main substance in the surface layer of the steel passivation film is FeOOH. As shown in Figure 1 (e), the ratios of FeOOH, FeO and Fe_3O_4 significantly change at 5 nm: FeOOH decreases from 66.2% to 49.8% and FeO and Fe_3O_4 increase to 37.5% and 12.7%, respectively. FeO and Fe_3O_4 are denser than FeOOH. According to the changes in the material composition, the passivation film is gradually denser from the outside to inside.

Table 4. XPS peak fitting data of Fe in the chloride solution

Depth/mm	Component	Binding energy/eV	Peak area/	Relative content/%
0 nm	FeOOH	709.4	6215	66.2%
		723	3125	
		715.4	196.9	
		729	99	
	FeO	711.9	1430.6	28.4%
		725.5	719.3	
		719.9	287.1	
		733.5	144.1	
	Fe_3O_4	710.8	606.7	5.4%
		724.4	305.1	
		710.8	606.7	
		724.4	305.1	
5 nm	FeOOH	709.4	4215	49.8%
		723	312.5	
		715.4	196.9	
		729	99	
	FeO	711.9	2230.6	37.5%
		725.5	919.4	
		719.9	289.1	
		733.5	144.1	
	Fe_3O_4	710.8	1606.7	12.7%
		724.4	305.1	
		710.8	1006.7	
		724.4	625.3	

Figures 1 (c) and (f) show the XPS spectrum of N in the solution with 0.5% chloride and 1.5 $n(NO_2^-)/n(Cl^-)$, indicating that the content of N in the passivation film is relatively small. Figure 1 (c) shows the XPS spectrum of N at 0 nm, which is mainly composed of $-NH_2$ and NH_4^+ with proportions of 86.5% and 10.6%, respectively. This finding indicates that part of NH_3 is dissolved in the pore

solution to generate NH_4^+ when $NaNO_2$ and Fe react to generate NH_3. The XPS spectrum of N at 5 nm is shown in Figure 1 (f), which is mainly composed of -NH_2, NH_4^+ and N=, accounting for 45.8%, 35.7% and 18.5%, respectively. Combined with the reaction energy spectrum, the sudden increase in N= is related to the reaction of C in the steel. The area of N in Figure 1 (f) is larger than that in Figure 1 (c), indicating that the forward reaction of the equation is more obvious, which conforms to the situation in which the amount of Fe_3O_4 at 5 nm in Figures 1 (b) and (e) is more than that at 0 nm.

3.1.3 Effect of $n(NO_2^-)/n(Cl^-)$on the corrosion of the reinforcement

Figure 2 shows the anodic polarization curves of the reinforcement in simulated pore solutions with different mass concentrations of NaCl. The reinforcement is in the passivation state when the external potential changes little, but the pitting potential changes negatively, which is in accordance with the findings in the literature [18]. The pitting potential decreases with increasing chloride content, leading to a smaller passivation zone. The current increases rapidly when the potential exceeds the pitting value. The passivation film on the surface of the reinforcement is damaged locally, resulting in pitting corrosion. Therefore, it can be concluded that the corrosion of the steel reinforcement in chlorine-doped concrete is caused by the reduction in the passivation zone and the positive movement of the steel reinforcement surface potential over the pitting potential under certain electrochemical action. The higher the chloride content is, the smaller the range of the passivation zone. The potential can easily exceed the pitting potential under the action of a small polarization, leading to the corrosion of the steel reinforcement. Similar results were obtained for HRBF500 doped in chloride-containing solution [19].

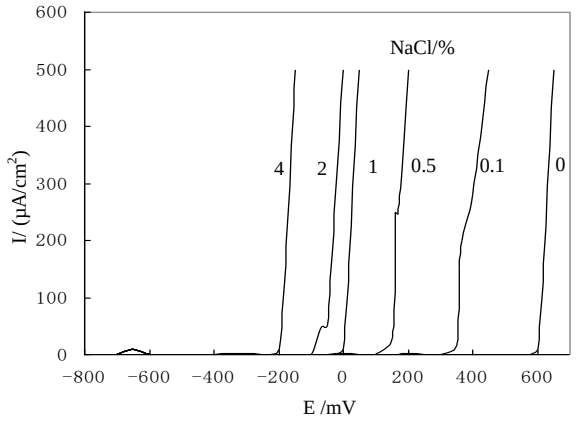

Figure 2. Polarization curves of the reinforcement in simulated pore solutions with different mass concentrations of NaCl

The anodic polarization curves in Figure 3 shows that sodium nitrite was added to the simulated pore solution containing sodium chloride, and the range of the passivation zone gradually increased with increasing sodium nitrite content. This finding is in accordance with the results reported in the literature [20-21], wherein nitrite can accelerate repassivation. Note that a larger $n(NO_2^-)/n(Cl^-)$

value is required to reach the same passivation zone with a higher content of chloride. When $n(NO_2^-)/n(Cl^-)$ is greater than 0.34, it is in the overpassivation range. This value is in the range reported in the literature [21]. The $n(NO_2^-)/n(Cl^-)$ required to inhibit steel corrosion in a concrete simulated pore solution is smaller than that in actual concrete. This discrepancy occurs because, on the one hand, the surface of a steel bar in concrete is not uniform relative to the aqueous solution, which is easy to produce macro batteries. On the other hand, nitrite has a fast migration rate in aqueous solution and is easy to repair the damage of passivation film caused by chloride ions.

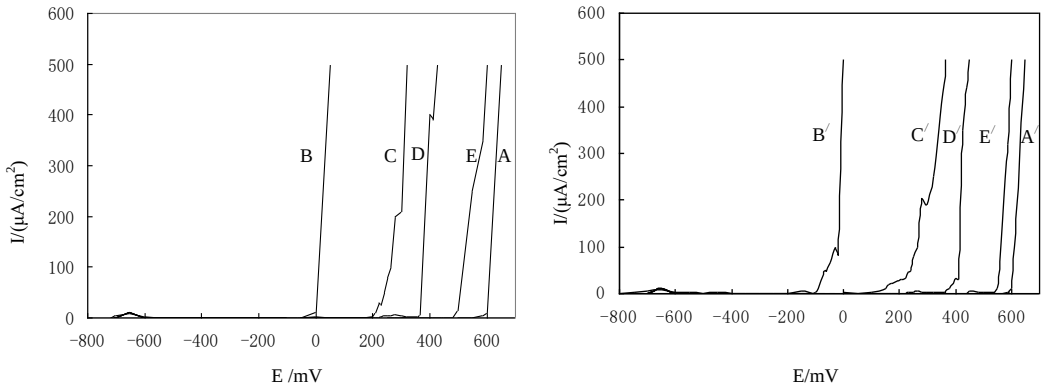

Figure 3. Polarization curves of the reinforcement in the $NaNO_2$ solution containing 1% and 2% NaCl

3.2 Microscopic characteristics of the passivation substance in the carbonated solution

3.2.1 XPS full-scan of the passivation substance in the carbonated solution

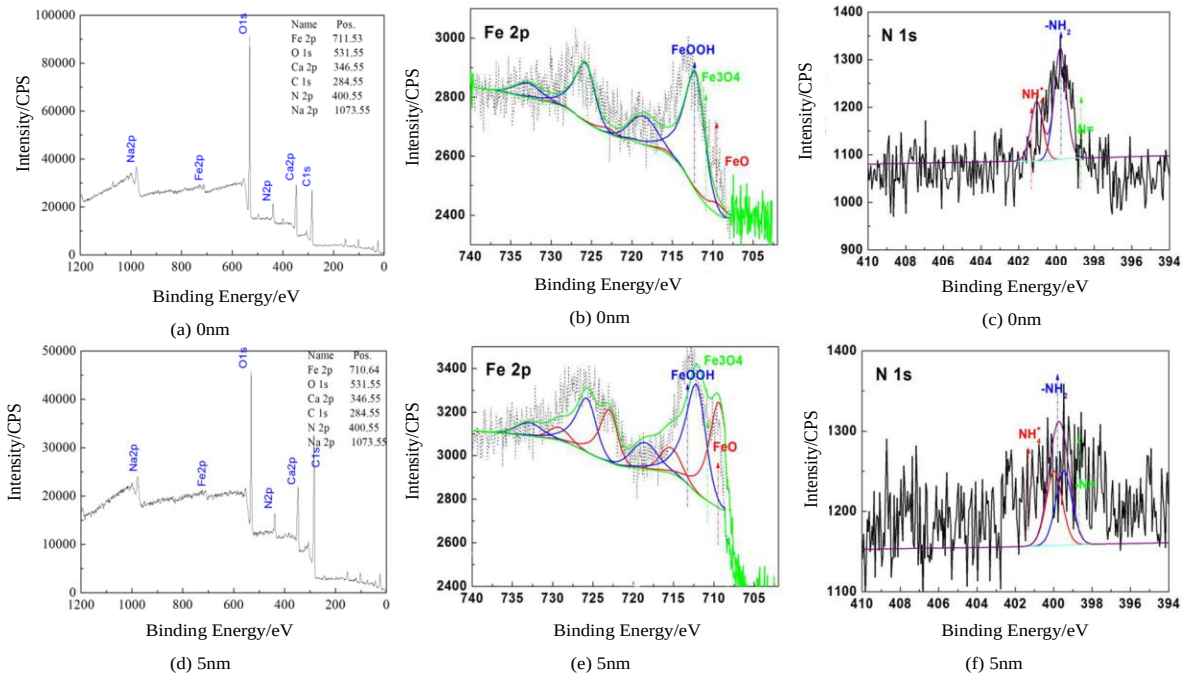

Figure 4. XPS full-scan spectrum diagrams showing Fe and N of the passivation film in the simulated carbonated solution at positions of 0 nm and 5 nm ($NaNO_2$=2%)

Figures 4 (a) and (d) show the XPS full-scan spectrum diagrams of the steel wafers after three months in the carbonated solution. The strong iron and oxygen peaks indicate that the main compositions of the steel passivation film in the solutions are mainly composed of iron oxides. The binding energies of Fe 2p at 0 nm and 5 nm in carbonated solution are 711.53 eV and 710.64 eV, respectively. Compared with the steel passivation film in the chloride solution, it can be seen that although the passivation films are mostly composed of iron oxides, the specific main compositions are different. During XPS analysis, FeO and Fe_3O_4 are mostly found at 5 nm, while they have relatively small peak areas at 0 nm with a larger peak area of FeOOH. These results indicated that the densification degree of the passivation film on the surface is weaker than that inside the carbonated solution[22].

3.2.2 XPS scanning images of Fe and N of the passivation film in the carbonated solution

Table 5. XPS peak fitting data of Fe in the carbonated solution

Depth/mm	Component	Binding energy/eV	Peak area/	Relative content/%
0 nm	FeOOH	709.4	6215	64.7
		723	3125	
		715.4	196.9	
		729	99	
	FeO	711.9	1430.6	16.3
		725.5	719.3	
		719.9	287.1	
		733.5	144.1	
	Fe_3O_4	710.8	606.7	19
		724.4	305.1	
		710.8	606.7	
		724.4	305.1	
5 nm	FeOOH	709.4	4215	38.1
		723	312.5	
		715.4	196.9	
		729	99	
	FeO	711.9	2230.6	47.1
		725.5	919.4	
		719.9	289.1	
		733.5	144.1	
	Fe_3O_4	710.8	1606.7	14.8
		724.4	305.1	
		710.8	1006.7	
		724.4	625.3	

Figures 4 (b) and (e) show the XPS spectrum of Fe in the solution with 2% NO_2^- and pH=9.7. Figure 4 (b) shows the XPS spectrum of Fe at 0 nm, which is mainly composed of FeOOH, FeO and Fe_3O_4, with proportions of 64.7%, 16.3%, and 19%, respectively. This finding indicates that the main component in the surface layer of the steel passivation film is mainly FeOOH [1]. As shown in Figure 4 (e), the ratio of FeOOH, FeO and Fe_3O_4 significantly changes at 5 nm: FeOOH decreases from 64.7% to 38.1% and FeO and Fe_3O_4 increase to 47.1% and 14.8%, respectively. These results indicate

that the passivation film became gradually denser from the outside to the inside. The XPS peak fitting data of Fe on the surface of the steel in carbonated solution is shown in Table 5.

Figures 4 (c) and (f) show the XPS spectrum of N in the solution with nitrite content of 2% and a pH of 9.7. The XPS diagram data presented by N fluctuate obviously, indicating that the overall content of this element in the steel wafers is low. By comparing the XPS spectrum of N at 0 nm and 5 nm, it can be seen that N= suddenly increased at 5 nm, indicating that some nitrite ions reacted with the surface of the reinforcement to generate the N=C binding compound.

3.3 Microscopic characteristics of the passivation substance in the compound solution

3.3.1 XPS full-scan of the passivation substance in the compound solution

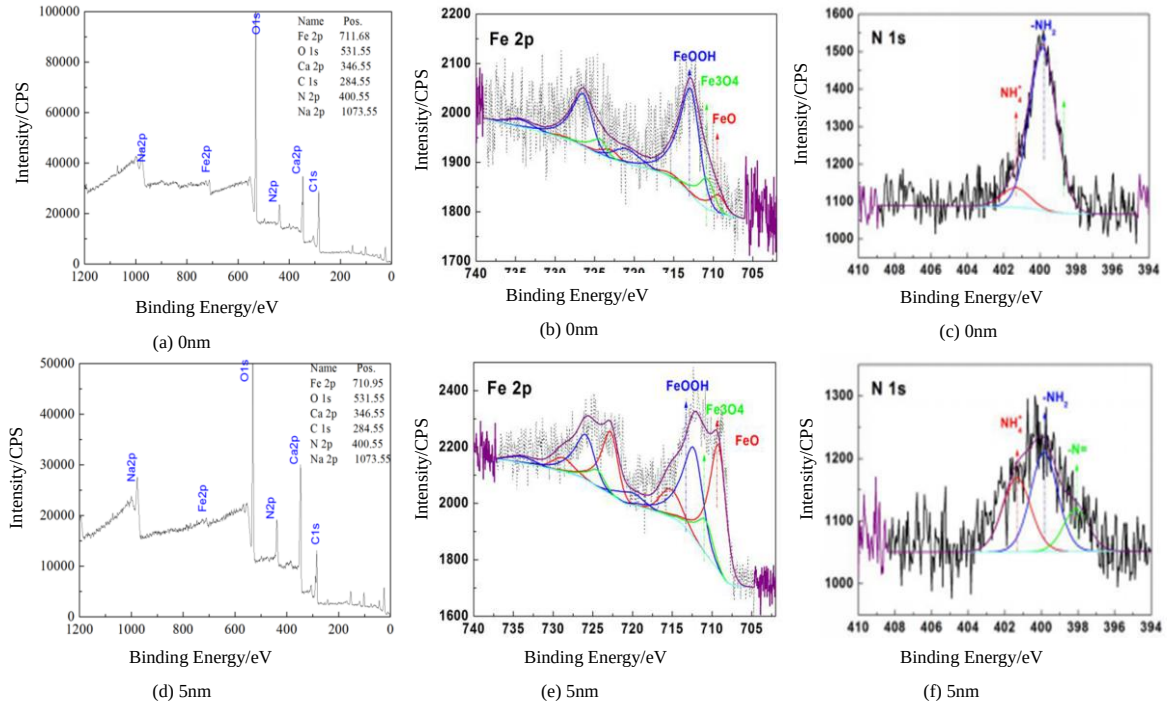

Figure 5. XPS full-scan spectrum diagrams showing Fe and N of the passivation film in the simulated solution combined with carbonation and chloride at positions of 0 nm and 5 nm ($n(NO_2^-)/n(Cl^-)=2$)

Figures 5 (a) and (d) are the XPS full-scan spectrum diagrams of the steel wafers after three months in the compound solution. It is also shown that the main composition of the passivation film on the surface of the steel wafers in the compound solution with nitrite ions is still iron oxides. Under these conditions, the binding energies of Fe 2p at 0 nm and 5 nm are 711.68 eV and 710.95 eV, respectively. This finding indicates that although the passivation film compositions in the three different solutions are all iron oxides, the specific main components are different, and they all show gradual densification from the outside to the inside [23]. A comparison between Table 4 and Table 6 shows that the binding energy of iron at 5 nm is higher than that at 0 nm, indicating that the iron oxide

increases and the densification of steel passivation film gradually increases in the interior, providing a good rust resistance effect. Combined with the XPS analysis in Figures 1, 4, and 5, the passivation film at 5 nm is mostly FeO and Fe_3O_4, which become the main protective layer of the steel. The peak area of FeO and Fe_3O_4 on the surface is small, and the peak area of FeOOH is large, indicating that the density of the passivation film is relatively weak compared with the density in the interior.

3.3.2 XPS scanning images of Fe and N of the passivation film in the compound solution

Figures 5 (b) and (e) show the XPS spectrum of Fe in the compound solution with 0.5% chloride, $n(NO_2^-)/n(Cl^-)$ =2 and pH=9.7. Figure 5 (b) shows the XPS spectrum of Fe at 0 nm, which is mainly composed of FeOOH, FeO and Fe_3O_4 with proportions of 74.7%, 11.3%, and 14%, respectively. This finding indicates that the surface layer of the passivation film is mainly dominated by FeOOH. As shown in Figure 5 (e), the ratios of FeOOH, FeO and Fe_3O_4 change significantly: FeOOH decreases from 74.7% to 40.1% and FeO and Fe_3O_4 increase to 50.1% and 9.8%, respectively. The content of FeO and Fe_3O_4 in the passivation film increases and that of FeOOH decreases obviously. It can be seen that when the ratio of $n(NO_2^-/n(Cl^-)$ increases, FeO and Fe_3O_4 increase faster in the interior, thereby slowing the corrosion of chloride [23]. The XPS peak fitting data of Fe on the surface of the steel corrosion in the compound solution is shown in Table 5.

Table 6. XPS peak fitting data of Fe in the compound solution

Depth/mm	Component	Binding energy/eV	Peak area	Relative content/%
0 nm	FeOOH	709.4	6215	74.7
		723	3125	
		715.4	196.9	
		729	99	
	FeO	711.9	1430.6	11.3
		725.5	719.3	
		719.9	287.1	
		733.5	144.1	
	Fe_3O_4	710.8	606.7	14
		724.4	305.1	
		710.8	606.7	
		724.4	305.1	
5 nm	FeOOH	709.4	4215	40.1
		723	312.5	
		715.4	196.9	
		729	99	
	FeO	711.9	2230.6	50.1
		725.5	919.4	
		719.9	289.1	
		733.5	144.1	
	Fe_3O_4	710.8	1606.7	9.8
		724.4	305.1	
		710.8	1006.7	
		724.4	625.3	

Figures 5 (c) and (f) show the XPS spectrum of N in the compound solution with 0.5% chloride and $n(NO_2^-)/n(Cl^-)$ =2. As shown in Figure 5 (c), this spectrum is mainly composed of $-NH_2$ and NH_4^+ with proportions of 70.5% and 29.7%, respectively. This finding indicates that when $NaNO_2$ and Fe

react to generate NH_3, some NH_3 is dissolved in the pore solution to generate NH_4^+. The amount of NH_4^+ generated is significantly higher than that in Figures 1 (c) and (f), indicating that when the molar ratio of $n(NO_2^-)/n(Cl^-)$ increased, it was helpful for the reaction equation to move to the right and promote the formation of the passivation film. In Figure 5 (f), the passivation film at 5 nm is mainly composed of $-NH_2$, NH_4^+ and N= with ratios of 39.8%, 18.6% and 41.57%, respectively, indicating that the N=C generated in the passivation film increases rapidly under this condition. The passivation film contains the products of N= and Fe when in the presence of a large amount of $NaNO_2$. The area of N in Figure 5 (f) is larger than that in Figure 4 (f), indicating that the forward reaction of the equation is more obvious, which conforms to the situation in which the amount of Fe_3O_4 at 5 nm of the steel wafers in Figure 5 is more than that at 0 nm.

3.4 XRD analysis of the passivation substance

Figures 6 (a)~(c) show the XRD spectrum of the passivation substance on the surface of the steel in the chloride solution, carbonated solution and the compound solution with sodium nitrite. There are two sets of obvious convex shapes for the peaks at 44.6° and 64.9° in Figure 6 (a), which were determined to be iron diffraction peaks after testing using a standard card of the X-ray diffraction spectrum. Elemental iron was detected in the chloride solution, indicating that a complete passivation film has not been formed under this condition, and some of them are without passivation. Except for two groups of obvious convex peaks, an analysis of other peaks shows that the passivation film on the surface of the steel wafers also contains ferrous hydroxide and ferric oxide in the solution with chloride.

There are three sets of obvious convex shapes for the peaks at 36.8°, 44.7° and 65.1° in Figure 6 (b), which were determined to be Fe_3O_4 diffraction peaks after testing using a standard card of the X-ray diffraction spectrum. A comparison to Figure 6 (a) shows that there are multiple subpeaks with a strong energy spectrum in this XRD spectrum. Iron hydroxide and ferric oxide also existed in the passivation film on the steel wafers in the carbonated solution mixed with nitrite.

Comparing Figure 6 (c) with Figures 6 (a) and (b), every peak is relatively more apparent, of which the main diffraction peaks were determined to be FeOOH. FeOOH was distributed at peak angles 2θ of 21.2°, 34.7°, 36.6°, 47.3°, 53.2°, 59.0°, and 61.3°. $FeCl_3$ and Fe_3O_4 were also present in the passivation film. The peak angles 2θ of $FeCl_3$ are 30.7° and 33.3°, and those of Fe_3O_4 are 30.1°, 35.4°, and 43.1°. These finding show that the compound effect of carbonation and chloride salt is not conducive to forming a complete passivation film, which is consistent with the results reported in the literature [9].

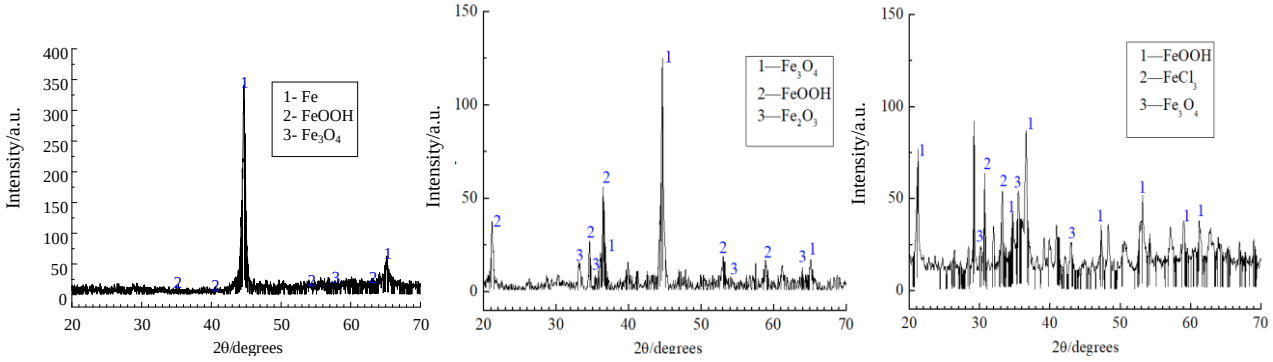

(a) chloride solution (b) carbonated solution (c) complex solution

Figure 6. XRD spectra of the passivation films in the three simulated solutions

3.5 Analysis of the passivation film formation process in the pore solution

By analyzing the XPS and XRD spectra above, the structural characteristics of the passivation substance on the surface of the steel in the different simulated solutions with nitrite were obtained. The passivation film of the steel in the solutions with nitrite is mainly composed of Fe_3O_4, and the content of the inner layer at 5 nm is greater than that at 0 nm. The formation process of Fe_3O_4 in the passivation film in the simulated pore solution with nitrite is as follows[24]:

$$3Fe + NaNO_2 + 5NaOH \rightleftharpoons 3Na_2FeO_2 + NH_3\uparrow + H_2O \quad (1)$$

$$6Na_2FeO_2 + NaNO_2 + 5H_2O \rightleftharpoons 3(NaFeO_2)_2 + NH_3\uparrow + 7NaOH \quad (2)$$

$$Na_2FeO_2 + (NaFeO_2)_2 + 2H_2O \rightleftharpoons Fe_3O_4 + 4NaOH \quad (3)$$

Ordinary carbon steel has a reversible reaction between Fe and $NaNO_2$ under an alkaline environment, and the intermediate product Na_2FeO_2, NH_3 and water are generated. When a sufficient amount of $NaNO_2$ is used, it will have reversible reactions with Na_2FeO_2 to generate $(NaFeO2)_2$, NH_3 and NaOH. Finally, Fe_3O_4 is formed in the solution when the amount of $(NaFeO_2)_2$ and Na_2FeO_2 is sufficient. However, the solubility of Fe_3O_4 is very low. When the forward reaction continues to make Fe_3O_4 reach the saturated concentration, the crystal precipitates out and finally forms a stable passivation film. Many previous studies have identified the components of passive films in chloride-containing solutions [25-26] but without comparison with carbonated and complex solutions.

The presence of FeOOH in the XPS analysis was due to the complete passivation film formed on the surface of steel preventing the reaction between the "outside" solution and Fe inside the passivation film. In addition, $(NaFeO_2)_2$ in the solution is easily hydrolyzed into $Fe(OH)_3$. Hydration products FeOOH accumulate in the outer layer of the passivation film and gradually form the "two-layer structure".

4. CONCLUSIONS

(1) In three simulated solutions with $NaNO_2$, steels present different degrees of corrosion under the effect of chloride and carbonation. In the chloride solution, a complete passivation film was formed

when $n(NO_2^-)/n(Cl^-)=1.5$. In the carbonated solution, the surface of the steel bar formed a complete passivation film after being immersed in a solution with 3% nitrite for 3 months. The corrosion range of the steel wafers in the compound solution was the widest. The passivation effect of the steel was obvious, and the surface was shiny when $n(NO_2^-)/n(Cl^-)=2.0$.

(2) In the simulated solution with $NaNO_2$, the main composition of the steel passivation film was FeOOH, FeO and Fe_3O_4, and the outer layer was mainly FeOOH, with FeO and Fe_3O_4 in relatively lower proportions. In the inner layer, FeO and Fe_3O_4 were predominant, and the content of FeO and Fe_3O_4 increased with increasing $NaNO_2$. The presence of FeOOH in the XPS analysis was due to the complete passivation film formed on the surface of steel preventing the reaction between the "outside" solution and the Fe inside the passivation film. $(NaFeO_2)_2$ in the solution was easily hydrolyzed into $Fe(OH)_3$. Hydration products FeOOH accumulated in the outer layer of the passivation film and gradually formed the "two-layer structure".

(3) Sodium nitrite increased the passivation range of the steel bars in the simulated pore solution with chloride, which can effectively prevent the corrosion of steel reinforcement caused by chloride ions. The higher the chloride ion content in the simulated pore solution was, the larger the molar ratio required to reach the same range of passivation zone. $NaNO_2$ does not participate in the composition of the passivation substance but takes part in the reaction process of generating the passivation substance, producing two intermediate products: $(NaFeO_2)_2$ and Na_2FeO_2. Fe_3O_4 was generated after the reaction of these two substances, and this was a slow dynamic equilibrium process that can control the thickness of the passivation film by changing the content of the reaction substances.

ACKNOWLEDGMENTS

This work was sponsored by the National Natural Science Foundation of China (51778302, 51878360) and the K.C. Wong Magna Fund at Ningbo University.

.

References

1. B. Qiao, R. G. Gui and C. J. Lin, *Acta Metall. Sin.*, 46 (2010) 245.
2. R.A. Medeiros-Junior, M.G. Lima, M.G., P.C. Brito and M.H.F. Medeiros, *Ocean Eng.*, 103 (2015) 78.
3. A. Poursaee, *Concr. Res. Lett.*, 1 (2010) 90.
4. S. H. Liu, J. J. Wang, H. B. Zhang, X. M. Guan, M. Qiu and Z. Z. Duo, *J. Wuhan Univ. Technol*, 34 (2019) 122.
5. J. Lu, W. S. Li and J. L. Luo, *Corros. Eng. Sci. Techn.*, 43 (2008) 208.
6. L. Liu, Y. Z. Xu, X. N. Wang, L. M. He and Y. Huang, *Mater. Rev.*, 31 (2017) 119.
7. M. Cabrini, F. Fontana, S. Lorenzi, T. Pastore and S. Pellegrini, *J. chem.,* (2015) 1.
8. Z. H. Dong, W. Shi and X. P. Guo, *Acta Phys-chim. Sin.*, 27 (2011) 127.
9. C. Resende, V. H. M. Silva, P. B. Martelli and A. H. S. Bueno, *Rev. Virtual Quim.*, 10 (2018) 1546.
10. N. Holmes, R. O.' Brien and P. A. M. Basheer, *Mater. Struc.*, 47 (2014) 1531.
11. D. M. Shen, *Int. J. Electrochem. Sci.*, 12 (2017) 4183.
12. J. Z. Liu, F. Xing and Z. M. He, *J. Chin. Ceram. Soc.*, 38 (2010) 615.

13. Z. Y. Ai, W. Sun and J. Y. Jiang, *Mater. Rev.*, 30 (2016) 92.
14. P. Ghods, O. B. Lsgor and J. R. Brown, *Appl. Surf. Sci.*, 257 (2011) 4669.
15. R. Blair, B. Pesic, J. Kline, I. Ehrsam and K. Raja, *Acta Metall. Sin-Engl.*, 30 (2017) 376.
16. H. L. Ye, Y. Tian and N. G. Jin, *Constr. Build. Mater.*, 47 (2013) 66.
17. J. Z. Liu, M. F. Ba, Y. G. Du, Z. M. He and J. B. Chen, *Constr. Build. Mater.*, 122 (2016) 619.
18. X. F. Yu, B. K. Sun, A. D. Lu, T. Wang, H. C. Zhang and H. S. Fan, *Corros. & Prot.*, 35 (2014) 18.
19. B. L. Lin and Y. Y. Xu, *Int. J. Electrochem. Sci.,* 11 (2016) 3824.
20. Z. H. Dong, W. Shi and X. P. Guo, *Corros. Sci.*, 53 (2011) 1322.
21. M. B. Valcarce, Z. C. López and M. Vázquez, *J. Electrochem. Soc.*, 159 (2012) 244.
22. W. Chen, R. G. Du, R. G. Hu, H. Y. Shi, Y. F. Zhu and C. J. Lin, *Acta Metall. Sin.*, 47(2011) 735.
23. Y. T. Tan, S. L. Wijesinghe and D. J. Blackwood, *J. Electrochem. Soc.*, 163(2016) 649.
24. J. Z. Liu, J. D. Geng, M. F. Ba, Z. M. He and Y. S. Li, *J. Build. Mater.*, 1 (2018) 1.
25. J. J. Shi and W. Sun. *Int. J. Min. Met. Mater.*, 19 (2012) 38.
26. Y. B. Tang, *Anti-Corros. Method. M.*, 64 (2017) 265.